# Density-functional study for the oligomers of poly(*para*-phenylene): Band structures and dielectric tensors

Peter Puschnig and Claudia Ambrosch-Draxl
*Institut für Theoretische Physik, Universität Graz, Universitätsplatz 5, A-8010, Austria*
(Received 11 May 1999)

The electronic and optical properties of the oligomers of poly(*para*-phenylene) (PPP) in their crystalline phases are calculated. In particular, the 2-, 3-, 4-, and the technically most important 6-unit oligomer *para*-hexaphenylene (6P) are considered. The electronic band structures are compared with the corresponding molecular orbitals in isolated molecules and the effect of intermolecular interactions is discussed. Connections between previous studies on the band structure of three-dimensional PPP and the present work are established. From the quasiparticle band structures the dielectric tensors are calculated and discussed also with respect to the corresponding transitions in the isolated molecules. [S0163-1829(99)04935-8]

## I. INTRODUCTION

During the past twenty years, conjugated polymers have attracted steadily growing interest, both experimental as well as theoretical. Electroluminescent devices with conjugated molecules as active materials represent one big area of applied scientific research on organic molecules.[1,2] Phenylene based materials are especially interesting on account of their high quantum efficiency and blue luminescence. A light emitting diode (LED) based on poly(*para*-phenylene) was demonstrated to produce intense blue light.[3] And devices with *para*-hexaphenylene (6P)—an oligomer of PPP containing six phenyl rings—as active layers have been shown to emit polarized light in a highly controlled way.[4] Moreover, such devices open the possibility to convert the emitted blue light into other colors; this way the working principle of future flat panel color displays was demonstrated.[5] In order to improve the performance of existing devices and to design more efficient ones, it is important to understand the electronic, optical and structural properties of the electroactive materials.

Among the methods to describe conjugated polymers on a microscopic level the solid state approach based on density functional theory (DFT) is not widely used. This is partly due to the computational challenge in handling unit cells with a large number of atoms, but also due to the success of competing theories. Quantum chemical calculations on finite isolated oligomers have been proven to accurately characterize ground state as well as excited state geometries and transition energies.[6–8] And among physical theories the Su-Schrieffer-Heeger model Hamiltonian[9] (and modifications of it[10]) successfully described nonlinear localized excitations in an isolated one-dimensional polymer chain, i.e., polarons or solitons for degenerate ground state polymers. But interactions with neighboring molecules—though inherently present in the solid state—are not accounted for in these two theoretical approaches. Indeed, fully three-dimensional (3D) DFT calculations for polyacetylene[11] have shown that interchain interactions destabilize the formation of nonlinear localized excitations (polarons, bipolarons) and a similar behavior can be deduced from calculations on 3D PPP (Refs. 12,13) and poly(*para*-phenylene-vinylene).[14]

In contrast to the assumption of perfect crystallinity in 3D DFT calculations, real samples of polymers show a distribution of various conjugation lengths, and the limited crystalline ordering suppresses the interchain interactions. Oligomers, on the contrary, can be obtained in high purity and with a very well ordered structure thus setting up defined intermolecular interactions. The oligomer 6P can be manufactured in a very pure form and highly oriented films can be obtained from it by vacuum evaporation techniques. Thus, the intermolecular interactions in such samples are very well defined and comparison with DFT calculations for the crystalline material are appropriate. Moreover, it is possible to influence the orientation of the molecules within the film by suitable film preparation conditions.[15] This is also true for shorter oligomers of PPP as was demonstrated for terphenyl (3P) and quaterphenyl (4P).[16] These highly ordered films open the possibility to experimentally confirm the theoretically predicted anisotropy in the electronic and optical properties.[17]

Within this work, these properties are calculated for the PPP oligomers from first principles. To our knowledge, the calculations presented here are the first ones for the oligomeric systems taking into account the full three-dimensionality of the materials in the solid state. Thus, the results contribute to clarify the role of intermolecular interactions in polymeric and oligomeric systems.

The paper is organized as follows. In Sec. II, the theoretical methods are described, followed by a discussion of the crystal structures of the oligophenylenes at room temperature. The electronic band structures of 2P, 3P, 4P, and 6P are presented in Sec. IV, where we analyze in detail the calculated band gaps and dispersions, the relations to molecular states of isolated oligophenylenes and the role of intermolecular interactions. In the next section, the dielectric tensors calculated from the Kohn-Sham orbitals are discussed. Finally a conclusion is given.

## II. METHODS

### A. Computational details

All calculations have been carried out with the linearized augmented plane wave (LAPW) method utilizing the WIEN97

 

code.[18] For exchange and correlation effects, the local density approximation (LDA) as well as a generalized gradient approximation (GGA) were applied. In the first case, the parameterization of Ceperly and Alder data[19] has been used according to Ref. 20. However, all calculations—if not mentioned explicitly—have been carried out with the PBE-GGA potential.[21]

A parameter which crucially determines the accuracy of any physical quantity calculated within the LAPW method is the number of basis functions included to diagonalize the Hamiltonian matrix, which in turn is chosen by $RK_{\max}$: the product of the muffin-tin radius and the largest reciprocal lattice vector in the plane wave expansion. For the carbon atoms $RK_{\max}$ of 6.0 has proven to be sufficient, resulting in matrix sizes of 4600, 6700, 8000, and 10 000 for 2P, 3P, 4P, and 6P, respectively.

The Brillouin zone (BZ) integration is performed according to the tetrahedron method. During the self-consistency cycle, 4 $k$ points in the irreducible BZ (IBZ) have been used. For the calculation of the dielectric function 280, 200, 140, and 105 points in the IBZ have been considered for 2P, 3P, 4P, and 6P, respectively.

### B. The dielectric function

From the knowledge of the single-particle orbitals and energies approximated by the solutions of the Kohn-Sham equations, the dielectric tensor $\varepsilon$ is computed. It is a well known fact that DFT calculations notoriously underestimate the band gaps of semiconductors. Fortunately, calculations of the electron self-energies have revealed that the true quasiparticle bands differ from the LDA bands for many materials by a **k**-independent rigid upward shift $\Delta_c$ of the conduction bands[22,23] (scissors operator). However, a simple shift of $E_{c\mathbf{k}}$ would yield too small values for the dielectric tensor components on account of the relation $\mathrm{Im}(\varepsilon)\sim 1/\omega^2$. It was shown that a rigorous treatment of the nonlocality of the self-energy operator requires a rescaling of the matrix elements.[24] According to this, the imaginary part of the dielectric tensor $\varepsilon_{ij}$ in the long-wavelength limit, is given by

$$\mathrm{Im}\,\varepsilon_{ij}(\omega)=\frac{4\pi^2e^2}{m^2(\omega-\Delta_c/\hbar)^2V}\sum_{v,c,\mathbf{k}}\langle v_{\mathbf{k}}|p_j|c_{\mathbf{k}}\rangle\langle c_{\mathbf{k}}|p_i|v_{\mathbf{k}}\rangle \times\delta(E_{c\mathbf{k}}+\Delta_c-E_{v\mathbf{k}}-\hbar\omega). \quad (2.1)$$

Here $|c_{\mathbf{k}}\rangle$ and $|v_{\mathbf{k}}\rangle$ are approximated by the Kohn-Sham orbitals with wave vector **k** for conduction and valence bands, respectively. $E_{c\mathbf{k}}$, $E_{v\mathbf{k}}$ are the corresponding band energies, and $p_i$ the Cartesian components of the momentum operator. $m$ denotes the free electron mass, $e$ the electron charge, $\omega$ the frequency, and $V$ the unit cell volume.

## III. CRYSTAL STRUCTURES

In the gaseous state the oligophenylenes are nonplanar molecules with alternating torsion angles between adjacent phenyl rings. This torsion angle ranges from 44° for biphenyl[25] to 30°–40° for the longer oligomers.[7] The interring torsion is the consequence of two competing forces: on the one hand the $\pi$-electron system of the carbons at the interring position tends to planarize the molecule, on the other hand the electrostatic repulsion of the positively charged *ortho*-hydrogens on neighboring rings forces the molecule into a nonplanar configuration. In the solid state we expect the interchain interactions (packing forces) to result in more planar molecules compared to the gas phase. For the infinite polymer, DFT calculations[12] have shown that the optimal interring torsion angle is 18° in agreement with experiment.[26] For the oligomers, on the other hand, x-ray and neutron diffraction experiments at room temperature reveal a planar configuration of the molecules in the monoclinic space group $P2_1/a$ with two molecules per unit cell (see Fig. 1). In the case of biphenyl (2P), one phenyl ring sets up the inequivalent atoms within one unit cell. The other half of the biphenyl molecule and the second molecule with its inversion center in the middle of the $ab$ plane are generated by the inversion, screw axis and glide plane operations of the $P2_1/a$ space group. In Table I the experimental values for the lattice parameters $a,b,c$ and the monoclinic angle $\beta$ are given. Additionally the angle $\zeta$ between the molecular axis and the $c$ axis is listed. Single crystal data for 2P (Ref. 27), 3P (Refs. 26,28), 4P (Ref. 29), and for the 5-, 6-, and 7-unit oligomers[30] are available from the literature. We observe that $a$ and $b$ remain almost constant as a function of the oligomer length. The small reduction in $a$ and $b$ with increasing oligomer length indicates a denser packing for longer molecules within the herring bone arrangement. The increase in $c$ for longer oligomers is simply a consequence of the

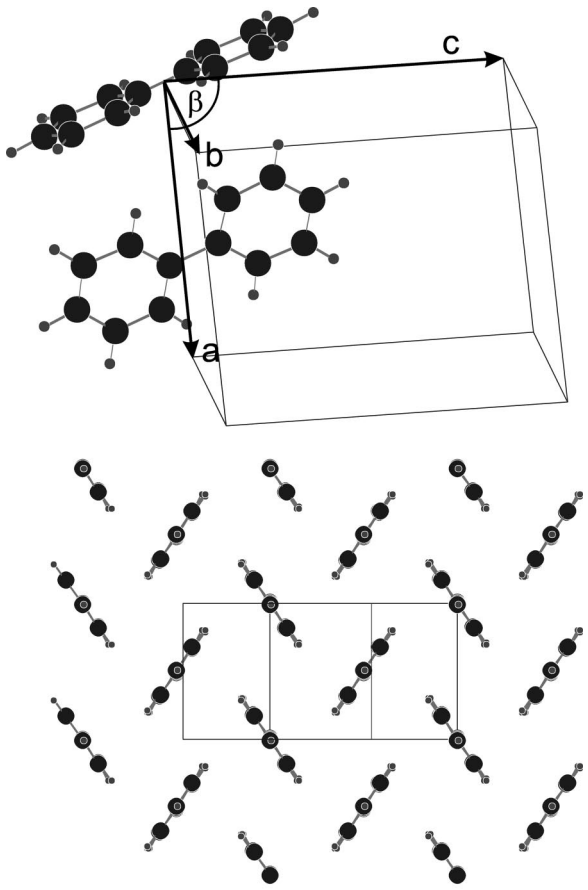


FIG. 1. Monoclinic unit cell of biphenyl with the two molecules per cell (top). Additionally, a projection of the crystal structure in the plane normal to the molecular axis shows the herring bone geometry (bottom).

TABLE I. Experimental unit cell parameters for some oligophenylenes at room temperature for the monoclinic space group $P2_1/a$. $\zeta$ is the angle between the molecular axis and the $c$ axis.

| Oligomer | $a$ (Å) | $b$ (Å) | $c$ (Å) | $\beta$ (°) | $\zeta$ (°) |
|---|---|---|---|---|---|
| biphenyl (Ref. 27) | 8.12(2) | 5.63(1) | 9.51 | 95.1 | 22.1 |
| $p$-terphenyl (Ref. 28) | 8.106(4) | 5.613(2) | 13.613(6) | 92.1(2) | 15.2 |
| $p$-quaterphenyl (Ref. 29) | 8.110(6) | 5.610(4) | 17.91(1) | 95.80(6) | 11.5 |
| $p$-quinquephenyl (Ref. 30) | 8.070(1) | 5.581(1) | 22.056(4) | 97.91(1) | |
| $p$-hexaphenyl (Ref. 30) | 8.091(3) | 5.568(1) | 26.241(5) | 98.17(2) | 25.5 |
| $p$-septiphenyl (Ref. 30) | 8.034(5) | 5.547(3) | 30.577(2) | 100.52(5) | |

growing length of molecules which are approximately parallel to $c$.

A closer look at the x-ray data shows, that the conformation of the molecules is planar only on average, and it is associated with high librational amplitudes around the long molecular axes.[28,25,31] The rings are assumed to librate in a double well potential and at low temperatures, when these rotations are frozen, a phase transition into a nonplanar conformation occurs, with the unit cell doubled containing four molecules.[32] Recent Raman studies of 6P under pressure also give rise to a nonplanar configuration at room temperature and normal pressure.[31] However, throughout this work we have considered only the high-temperature phase with coplanar oligo-phenylene molecules.

For the shorter oligomers, 2P, 3P, and 4P, we have taken the atomic positions obtained from x-ray diffraction experiments. Since the calculated atomic forces turned out to be moderate and could be neglected in a first approximation, we did not optimize the atomic positions. For 6P, however, calculations for both the experimental as well as for a geometry optimized structure were performed. The process of geometry optimization takes account of the atomic forces and shifts the atomic positions according to the direction and magnitude of the particular force in a damped oscillator scheme until all forces are vanishingly small.[33] A structure optimization starting with the experimental geometry proved to be necessary on account of the much larger forces acting on the atoms compared with the other oligomers. It turned out that the calculated band gaps of the two structures differ by 0.4 eV. Thus, in view of the technical importance of 6P the time consuming procedure of geometry optimization (in the order of one month on a vector computer) is justified. In Fig. 2 intraring as well as inter-ring $C$-$C$ bond lengths for the experimental and the geometry optimized structure of 6P are displayed. Theory predicts the rings to be much more symmetric as is the case for the experimental data for the shorter oligomers. Moreover, both the inter-ring as well as intraring bond lengths are in accordance with previous DFT calculations for PPP (Ref. 12) and with quantum chemical calculations for oligophenylenes,[7] respectively.

## IV. ELECTRONIC STRUCTURE

### A. From molecular states to crystal bands

Looking at the molecular orbitals (MO's) of biphenyl, we can see what type of energy bands can be expected in the solid state. To understand the electronic states of biphenyl schematically we think of it as consisting of two benzene molecules, and let the molecular states of biphenyl evolve from the benzene molecular states (see Fig. 3).[34] One can distinguish between $C\ p_\pi$ and $p_\sigma$ orbitals. Energetically, the $\pi$ orbitals constitute the highest occupied molecular orbital (HOMO) and the lowest unoccupied molecular orbital (LUMO). Benzene belongs to the $D_{6h}$ point group and taking the six carbon $\pi$ orbitals as basis functions the HOMO-1, HOMO, and LUMO belong to the $a_{2u}$, $e_{1g}$, and $e_{2u}$ irreducible representation of $D_{6h}$. The local symmetry of each of the benzene moieties in biphenyl changes from $D_{6h}$ to $C_{2v}$. Thus, each of the two doubly degenerate states $e_{1g}$ and $e_{2u}$ are now split up into $b_1$ and $a_2$ states. Combining the two benzene moieties into biphenyl with $D_{2h}$ symmetry results in the actual biphenyl MO's, for which the atomic orbital compositions of the highest six occupied and lowest four unoccupied MO's are displayed. The $1a_u$ and $1b_{1g}$ states of biphenyl, originating in the $a_2$ MO's of benzene, are close in energy, because the interaction across the interring

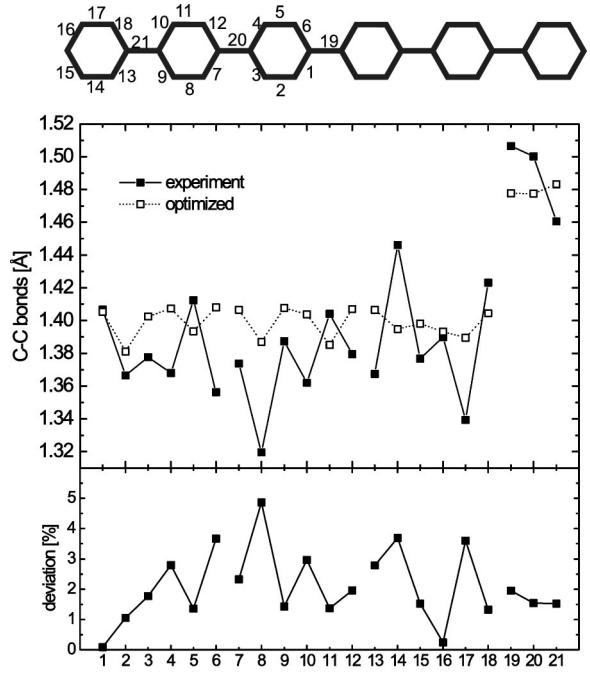


FIG. 2. The $C$-$C$ bond lengths in crystalline 6P for the experimental geometry (full symbols) and the DFT-optimized geometry (open symbols) are depicted in the upper panel. The relative deviation of the bond lengths in the two structures is displayed (lower panel). The labeling of the bond lengths is according to the schematic picture shown on top of the figure. The geometry for the right three rings is identical to the left ones by symmetry.

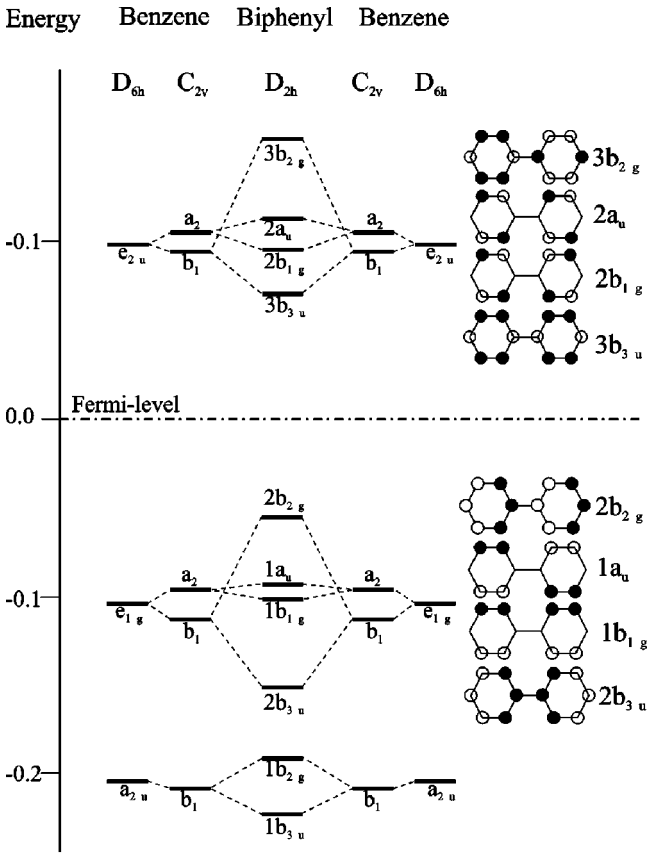


FIG. 3. Diagram showing the evolution of the molecular orbitals of biphenyl from the MO's of two benzene rings. According to a Hückel picture, the atomic orbital compositions of the top four HOMO's and lowest four LUMO's, respectively, are depicted. Filled (open) circles correspond to $p_\pi$ orbitals that have positive (negative) sign at one side of the molecular plane.

bridge is weak. These states are mainly *localized* at the benzene rings. On the other hand, the interaction of the $b_1$ benzene states forming the $2b_{3u}$ and $2b_{2g}$ states of biphenyl is large—so is their energetic separation. The corresponding wave functions are spread over the whole molecule (*delocalized* states).

### B. Band structures

The GGA band structures of 2P, 3P, 4P, and 6P are presented in Figs. 4 and 5. We start with a description of the electronic band structure of biphenyl. All states depicted in Fig. 3 for the isolated biphenyl molecule are doubled in the crystal on account of the herring-bone structure which has two molecules per unit cell. The splitting of the bands is a measure for the intermolecular interaction.

The eight top valence bands of crystalline biphenyl clearly resemble the molecular orbital picture. The two highest valence bands (VB's) originate from the $2b_{2g}$ MO of the biphenyl molecule. The next four lower lying bands are derived from the $1a_u$ and $1b_{1g}$ MO's, respectively, whereas the VB-6 and VB-7 evolve from the MO of $2b_{3u}$ symmetry. This assignment is confirmed by electron density plots of these valence bands (Fig. 6) when compared with the schematic molecular orbital pictures for the isolated biphenyl (Fig. 3). It is interesting to note that the band splittings due to

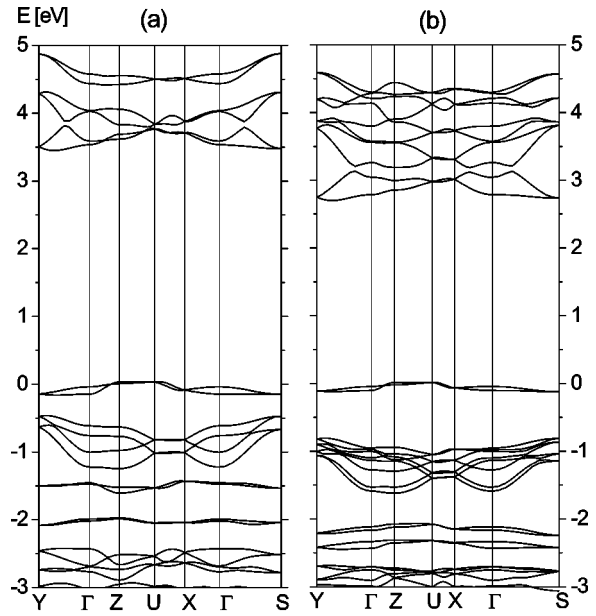


FIG. 4. Band structures of 2P (a) and 3P (b) along high symmetry directions in the reciprocal space. The band gaps have not been corrected for the self-energy of the conduction bands. $\Gamma Z$ is almost parallel to the long molecular axis, whereas $\Gamma X$ and $\Gamma Y$ are perpendicular to it.

intermolecular interactions are much larger for the $1a_u$ and $1b_{1g}$ symmetry bands (splitting of $\cong 0.4$ eV at $\Gamma$), whereas the interaction is much less (splitting of $\cong 0.08$ eV at $\Gamma$) for the $2b_{2g}$ and $2b_{3u}$ bands. The reason for this behavior can be deduced from the electron density plots in Fig. 6. The $2b_{2g}$ and $2b_{3u}$ states are mainly located at the molecular axis, thus the interaction with a neighboring molecule is small due to

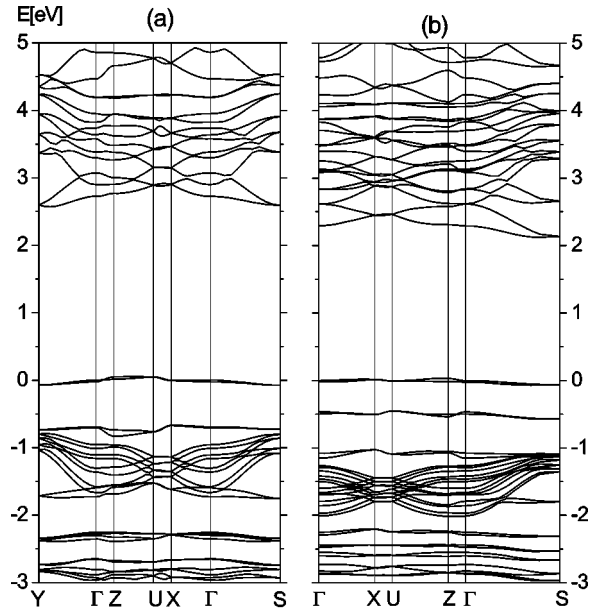


FIG. 5. Band structure of 4P (a) and 6P (b) along high symmetry directions in the reciprocal space. The results for 6P are obtained for the geometry optimized structure. The band gaps have not been corrected for the self-energy of the conduction bands. $\Gamma Z$ is almost parallel to the long molecular axis, whereas $\Gamma X$ and $\Gamma Y$ are perpendicular to it.

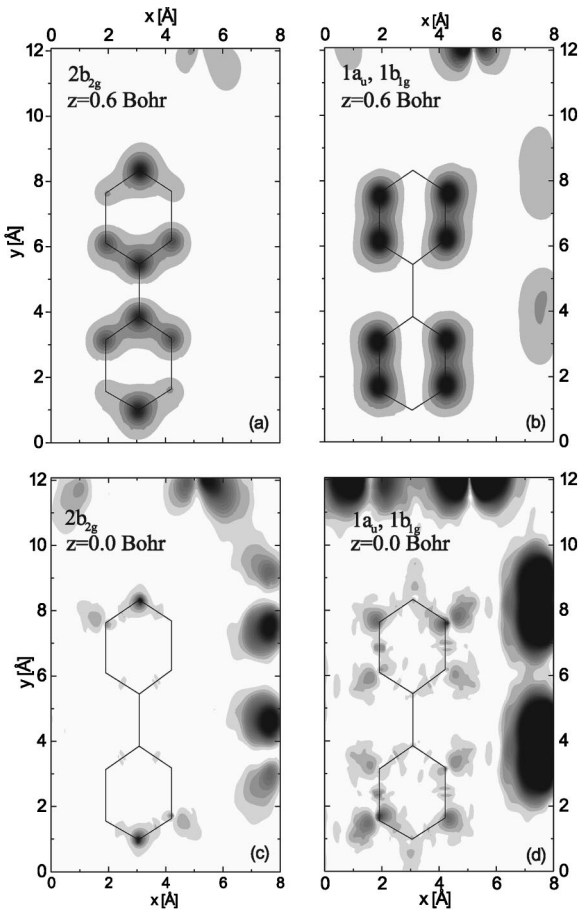


FIG. 6. Panels (a) and (b) show the electron density of the *delocalized* and *localized* valence bands of 2P, respectively, in a plane parallel to the molecular plane at a distance of 0.6 Bohr. Panels (c) and (d) display the electron density of the *delocalized* and *localized* bands, respectively, but now *in* the molecular plane.

their larger distance. On the other hand, the $1a_u$ and $1b_{1g}$ MO's are mainly located at the *ortho*-carbons and point approximately towards the hydrogens of the neighboring molecule, hence establishing a weak C-H bond. This bond is also the reason for the pronounced asymmetry between occupied and unoccupied bands. In a pure $\pi$ electron picture there would be perfect electron-hole symmetry: the unoccupied conduction bands are mirror bands of the occupied valence bands. On account of the intermolecular interaction the valence bands no longer have pure $\pi$ character and this symmetry is destroyed. A proof for this description can be seen in the lower panels of Fig. 6. There we have plotted the electron density of the bands derived from the $2b_{2g}$ MO (VB, VB-1) and those derived from the $1a_u$ and $1b_{1g}$ MO's (VB-2, -3, -4, -5) in the plane of the molecule. In a pure $\pi$ electron model the electron density in this plane should be equal to zero. The nonzero electron density as shown in Fig. 6 has two reasons: the experimental geometry of biphenyl is not perfectly planar,[27] thus some atoms have a finite distance from the average molecular plane. But more important, the electron density at the hydrogens explains the intermolecular interaction described above and also accounts for the different values of the band splittings for the top four valence bands.

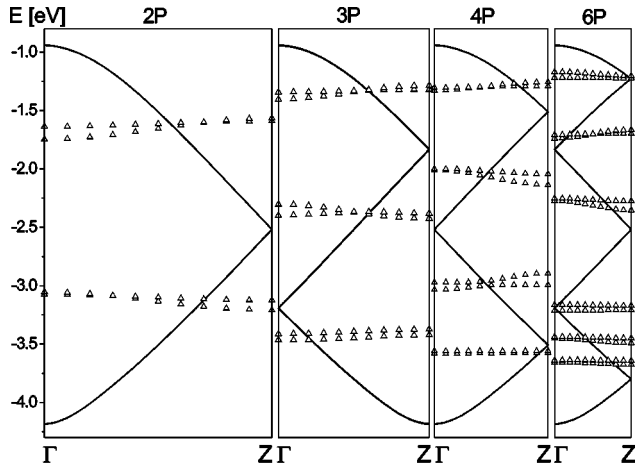


FIG. 7. The delocalized VB's of 2P, 3P, 4P, and 6P along $\Gamma Z$ are depicted (triangles). Additionally, these bands are compared with the delocalized VB of PPP (lines) parallel to the polymer axis. For better comparison with the oligomers the unit cell of PPP contains 2, 3, 4, and 6 rings when compared with 2P, 3P, 4P, and 6P, respectively.

Terphenyl consists of three phenyl rings. If we look at Fig. 3 once again we expect the following electronic states: three occupied $a_2$ and another three occupied $b_1$ benzene states form the six highest VB's of terphenyl. The three $a_2$ MO's form orbitals similar to the $1a_u$ and $1b_{1g}$ states of biphenyl. Consequently, the interaction across the inter-ring bridge is weak and the three MO's (six bands on account of the second molecule in the unit cell) lie close to each other. Similar to biphenyl, the intermolecular splitting of these bands is large ($\cong 0.45$ eV at $\Gamma$). The remaining three MO's of terphenyl are constructed from the $b_1$ states of benzene. Just as was the case for biphenyl, these states interact across the inter-ring bond and are thus separated by a total of about 2 eV with respect to each other. Again the intermolecular interaction destroys the symmetry between valence and conduction band states.

From what was said above, it should be clear what happens upon adding one more phenyl ring to end up with quaterphenyl or another three phenyl rings to end up with hexaphenyl. Indeed, the calculated band structures (see Fig. 5) support the qualitative picture developed above. In the case of quaterphenyl, the four $a_2$ benzene MO's form four MO's (eight VB's) that show little interaction across the interring bridge and consequently nearly no energetic separation. But again these bands show strong intermolecular interactions. The other four benzene states of $b_1$ form four largely (2.3 eV) separated MO's (eight valence bands, respectively). Finally, the electronic band structure of hexaphenyl can also be derived in the same manner from the MO's of benzene.

Although the description presented above nicely explains the principal features in the electronic structure of the oligomers, we want to interpret the calculated band structures in an additional way; i.e., starting with the band structure of PPP. In Fig. 7 the *delocalized* valence band of coplanar PPP along the polymer axis is depicted. It has a bandwidth of about 3 eV and is derived from the $b_1$ benzene states. For better comparison with the oligomers, the delocalized PPP band is drawn for a unit cell with 2, 3, 4, and 6 phenyl rings

TABLE II. Calculated bandwidth of the highest valence bands (VB) and lowest conduction bands (CB) of biphenyl, terphenyl, quaterphenyl, and hexaphenyl along the $\Gamma Z$, $\Gamma X$, and $\Gamma Y$ direction in reciprocal space.

| | Biphenyl | Terphenyl | Quaterphenyl | Hexaphenyl |
|---|---|---|---|---|
| | | bandwidth (eV) | | |
| VB: $\Gamma Z$ | 0.14 | 0.08 | 0.06 | 0.04 |
| VB: $\Gamma Y$ | 0.05 | 0.07 | 0.07 | 0.05 |
| VB: $\Gamma X$ | 0.11 | 0.03 | 0.02 | 0.02 |
| CB: $\Gamma Z$ | 0.08 | 0.08 | 0.05 | 0.02 |
| CB: $\Gamma Y$ | 0.31 | 0.35 | 0.40 | 0.40 |
| CB: $\Gamma X$ | 0.17 | 0.20 | 0.18 | 0.16 |

as repeat unit, thus with $\frac{1}{2}$, $\frac{1}{3}$, $\frac{1}{4}$, and $\frac{1}{6}$ length of the Brillouin zone along the chain direction. The PPP band (lines) is compared with the corresponding valence bands of 2P, 3P, 4P, and 6P along the molecular axis, respectively. We can see how the oligomer bands, upon increasing the oligomer length, gradually build up the top valence band of PPP. The total bandwidth of the delocalized levels (triangles) increases towards the PPP limit and at the same time the energetic distance between the single delocalized bands is reduced. There are still gaps between these bands because $\pi$ conjugation is only extended over a finite distance in the oligomer. The general picture described above is in accordance with the quasiband model of finite length oligomers.[35,36]

### C. Band gaps and dispersions

As described in the theory part, the conduction bands have to be corrected by a self-energy $\Delta_c$. We found $\Delta_c$ to be more or less equal for all oligomers. In accordance with previous findings for the self-energy of PPP ($\Delta_c = 1.2$),[12] it was taken to be $\Delta_c = 1.4$ eV for the LDA calculations and $\Delta_c = 1.3$ eV for the GGA results, respectively. Experimentally, the band gaps follow the so-called $1/n$ law.[17,37,38] The position of the first absorption peak shows a linear dependence as a function of the inverse oligomer length, where $n$ denotes the number of phenyl rings per molecule. Our results for the band gaps as a function of $n$, which are in agreement with the experimental data, have already been published elsewhere.[39] Qualitatively, a decreasing band gap with increasing oligomer length can be understood, if one considers the increasing total bandwidth of the VB's derived from the $b_1$ states of benzene. This bandwidth is 1.5, 2.0, 2.2, and 2.4 eV for 2P, 3P, 4P, and 6P, respectively, and approaches 3 eV for the infinite polymer (see discussion in the previous subsection).

Measurements of the electro-luminescence on oriented films of 6P suggest that the carrier mobility along the molecular axis is smaller than its counterpart perpendicular to it.[40] The carrier mobility is proportional to the effective mass which in turn is inversely proportional to the bandwidth of the considered band along a given direction. In Table II, these intermolecular bandwidths of the highest VB and the lowest CB for 2P, 3P, 4P, and 6P are listed for three different directions in the reciprocal space. $\Gamma Z$ is nearly parallel to the molecular axis, whereas $\Gamma X$ and $\Gamma Y$ are almost perpendicular to the molecular axis. The results for the highest VB (lowest CB), e.g., for 6P, of 0.04 (0.02) eV along $\Gamma Z$ and 0.05 (0.40) eV along $\Gamma Y$ are of the same order of magnitude and thus qualitatively support the experimental findings. Therefore, in contrast to what was found experimentally for infinite polymer chains, the carrier mobility for short oligomers is likely to be higher perpendicular to the long molecular axis than parallel to it.

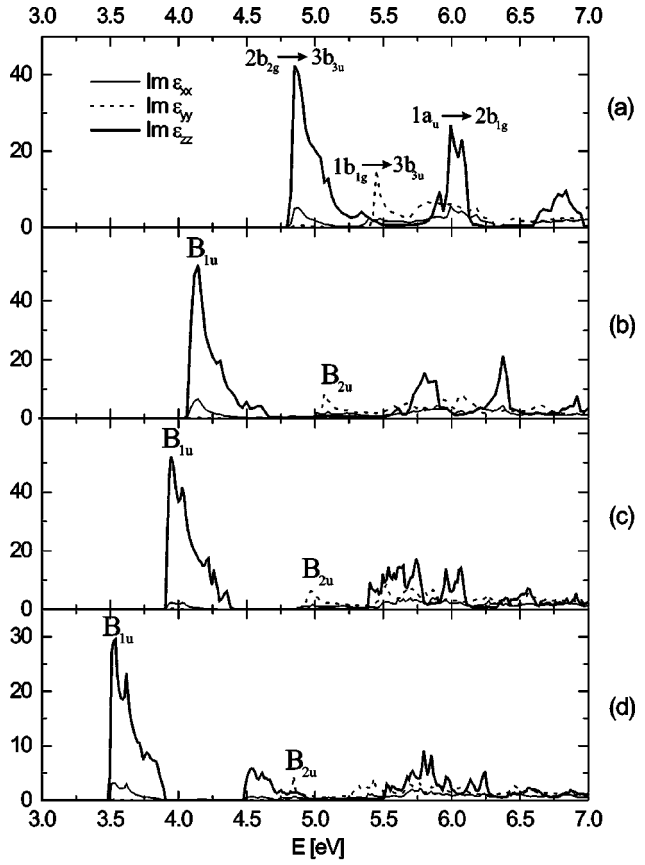


FIG. 8. The imaginary part of the DF for 2P (a), 3P (b), 4P (c), and 6P (d), respectively. The three diagonal components $\mathrm{Im}\,\varepsilon_{xx}$, $\mathrm{Im}\,\varepsilon_{yy}$, and $\mathrm{Im}\,\varepsilon_{zz}$ of the dielectric tensors are displayed. The results include a shift of $\Delta_c = 1.3$ eV accounting for the self-energy of the conduction bands. The symmetry of the main transitions is indicated in the MO notation as explained in the text.

## V. OPTICAL PROPERTIES

The dielectric tensor of a crystal with a monoclinic unit cell has four independent components, which are computed according to Eq. (2.1) from the band structures discussed in the previous section. The results for the 2-, 3-, 4-, and 6-unit oligomer are depicted in Fig. 8. The results already include a rigid upward shift $\Delta_c = 1.3$ eV accounting for the self-energy of the conduction bands. Similar to the procedure in the previous section about the electronic band structure, we want to discuss first, what type of optical excitations and polarizations we have to expect for an isolated biphenyl molecule and compare these qualitative considerations with the *ab initio* calculation of the dielectric function (DF) for crystalline biphenyl [Fig. 8(a)]. If we define the long molecular axis as the $z$ axis and the axis perpendicular to $z$ and in the plane of the molecule as the $y$ axis, then the dipole operator accounting for a polarization parallel to the $z(y)$ axis belongs to the

TABLE III. Electric dipole transitions of molecular biphenyl. The long molecular axis is parallel to $z$, the $y$ axis is normal to $z$ and in the plane of the molecule. The transitions are characterized according to the irreducible representations of the $D_{2h}$ point group of biphenyl.

| Representation | $B_{1u}$ | $B_{2u}$ | $B_{3g}$ | $A_g$ |
|---|---|---|---|---|
| Polarization | $z$ | $y$ | forbidden | forbidden |
| | $2b_{2g}\rightarrow 3b_{3u}$ | $1b_{1g}\rightarrow 3b_{3u}$ | $2b_{2g}\rightarrow 2b_{1g}$ | $1b_{1g}\rightarrow 2b_{1g}$ |
| | $1a_u\rightarrow 2b_{1g}$ | $2b_{2g}\rightarrow 2a_u$ | $1a_u\rightarrow 3b_{3u}$ | $1a_u\rightarrow 2a_u$ |
| | $1b_{1g}\rightarrow 2a_u$ | | | |

$B_{1u}(B_{2u})$ irreducible representation of $D_{2h}$. In Table III, the low-energy transitions of isolated biphenyl are listed. Transitions belonging to the $B_{3g}$ and $A_g$ representation are electric-dipole forbidden by symmetry. For an explanation of the molecular orbital terminology see Fig. 3. In summary it can be said, that transitions between two *delocalized* or between two *localized* levels are polarized in the $z$ direction, whereas transitions between localized and delocalized levels are allowed for polarizations along the $y$ direction.

The calculation of the imaginary part of the DF includes a sum over all possible valence $|v_{\mathbf{k}}\rangle$ and conduction band states $|c_{\mathbf{k}}\rangle$ and the resulting DF is a combination of all transitions between $|v_{\mathbf{k}}\rangle$ and $|c_{\mathbf{k}}\rangle$ [see Eq. (2.1)]. It is interesting to look at the contributions to the DF of particular band combinations and compare these to what has to be expected from an independent-molecule picture. In an isolated biphenyl molecule, the HOMO to LUMO transition is polarized parallel to the long molecular axis (see also Table III). In the crystal, the polarization of the lowest energy transition remains alMO'st the same. Hence there is only a small contribution to $\mathrm{Im}\,\varepsilon_{yy}$, and the ratio of $\mathrm{Im}\,\varepsilon_{zz}$ and $\mathrm{Im}\,\varepsilon_{xx}$ is related to the angle between the molecular axis and the long unit cell axis (Fig. 1). At about 0.6 eV higher energies the first ''delocalized-to-localized transitions'' appear. They set up the major part to the $xx$ and $yy$ component at this energy, but have almost no contribution to $\mathrm{Im}\,\varepsilon_{zz}$. Excitations that are electric-dipole forbidden in the molecule ($B_{3g}$ and $A_g$), become weakly allowed in the crystalline environment.

The dielectric functions of 3P, 4P, and 6P are similar to the DF of biphenyl. According to the $1/n$ law the lowest transition is red shifted. With increasing oligomer length, the first transition polarized perpendicular to the molecular axis shifts to higher energies with respect the lowest transition. The peaks in the $\mathrm{Im}\,\varepsilon_{yy}$ lie 0.6, 0.9, 1.0, and 1.2 eV above the absorption onset in 2P, 3P, 4P, and 6P, respectively. In addition the intensity of the perpendicular transition decreases.

## VI. CONCLUSIONS

We have performed first-principles calculations for the electronic and optical properties of oligophenylenes within the framework of density functional theory. In particular, the three-dimensional band structures and the dielectric tensors of biphenyl, terphenyl, quaterphenyl, and hexaphenyl in their crystalline form were calculated. Comparison of the band structures with the molecular states of the isolated oligophenylenes shows that the main character of the $\pi$ orbitals is preserved in the crystal. However, the intermolecular interactions lead to important modifications with respect to the isolated molecules. The band splittings due to the interaction of two neighboring molecules in the herring bone arrangement are in the order of $0.1-0.2$ eV for the *delocalized* bands, which set up the highest valence bands, and lowest conduction bands. The analogous value for the *localized* bands is somewhat bigger (0.4 eV), and can be explained by a larger overlap of the wave functions of two neighboring molecules in the latter case. In a first approximation, the dispersions of the top valence and lowest conduction band, respectively, can be taken as a measure for the carrier mobility. Analysis of these bands along directions *parallel* and *perpendicular* to the molecular axis shows, that the dispersion is higher for the perpendicular case, which can be understood by a stronger overlap of the wave functions within the herring bone layers rather than between them.

The dielectric tensors of 2P, 3P, 4P, and 6P reflect the pronounced anisotropy in the optical properties of the oligophenylene molecules. As for the isolated molecules, the lowest transition is polarized parallel to the long molecular axis. We find that the energy of this transition decreases linearly with the inverse oligomer length, but appears broadened (0.4 eV) on account of the finite bandwidths due to intermolecular interactions. For the first transition which is polarized perpendicular to the molecular axis, the increasing oligomer length results in a shift to higher energies with respect to the lowest transition, accompanied by a decrease in intensity.

[1] C. W. Tang and S. A. VanSlyke, Appl. Phys. Lett. **51**, 913 (1987).
[2] R. H. Friend and N. C. Greenham, in *Handbook of Conducting Polymers*, edited by J. R. R. T. A. Skotheim and R. L. Elsenbaumer (Marcel Dekker, New York, 1998).
[3] G. Grem, G. Leditzky, B. Ullrich, and G. Leising, Adv. Mater. **4**, 36 (1992).
[4] M. Era, T. Tsutsui, and S. Saito, Appl. Phys. Lett. **67**, 2436 (1995).
[5] S. Tasch, C. Brandstätter, F. Meghdadi, G. Leising, G. Froyer, and L. Althouel, Adv. Mater. **9**, 33 (1997).
[6] J. L. Bredas, R. R. Chance, R. Silbey, G. Nicolas, and P. Durand, J. Chem. Phys. **77**, 371 (1982).
[7] E. Zojer, J. Cornil, G. Leising, and J. L. Bredas, Phys. Rev. B **59**, 7957 (1999).
[8] J. Cornil, D. Beljonne, and J. L. Bredas, J. Chem. Phys. **103**, 834 (1995).

[9] W. P. Su, J. R. Schrieffer, and A. J. Heeger, Phys. Rev. B **22**, 2099 (1980).
[10] K. Fesser, A. R. Bishop, and D. K. Campbell, Phys. Rev. B **27**, 4804 (1983).
[11] P. Vogl and D. K. Campbell, Phys. Rev. B **41**, 12 797 (1990).
[12] C. Ambrosch-Draxl, J. A. Majewski, P. Vogl, and G. Leising, Phys. Rev. B **51**, 9668 (1995).
[13] C. Ambrosch-Draxl, J. A. Majewski, P. Vogl, G. Leising, R. Abt, and K. D. Aichholzer, Synth. Met. **69**, 411 (1995).
[14] P. G. D. Costa, R. G. Dandrea, and E. M. Conwell, Phys. Rev. B **47**, 1800 (1993).
[15] R. Resel, N. Koch, F. Meghdadi, G. Leising, W. Unzog, and K. Reichmann, Thin Solid Films **305**, 232 (1997).
[16] L. Althouel, R. Resel, N. Koch, F. Meghdadi, G. Froyer, and G. Leising, Synth. Met. **101**, 627 (1999).
[17] A. Niko, F. Meghdadi, C. Ambrosch-Draxl, P. Vogl, and G. Leising, Synth. Met. **76**, 177 (1996).
[18] P. Blaha, K. Schwarz, and J. Luitz, WIEN97, *A Full Potential Linearized Augmented Plane Wave Package for Calculating Crystal Properties* (Techn. Universität Wien, Austria, 1999).
[19] D. M. Ceperley and B. J. Alder, Phys. Rev. Lett. **45**, 566 (1980).
[20] J. P. Perdew and Y. Wang, Phys. Rev. B **45**, 13 244 (1992).
[21] J. P. Perdew, K. Burke, and M. Ernzerhof, Phys. Rev. Lett. **77**, 3865 (1996).
[22] X. Zhu and S. G. Louie, Phys. Rev. B **43**, 14 142 (1991).
[23] G. Brocks, P. J. Kelly, and R. Car, Synth. Met. **55**, 4243 (1993).
[24] R. Del Sole and R. Girlanda, Phys. Rev. B **48**, 11 789 (1993).
[25] J. L. Baudour, Acta Crystallogr. **47**, 935 (1991).
[26] J. L. Baudour, H. Cailleau, and W. B. Yelon, Acta Crystallogr. **33**, 1773 (1977).
[27] G.-P. Charbonneau and Y. Delugeard, Acta Crystallogr. **33**, 1586 (1977).
[28] H. M. Rietveld, E. N. Maslen, and C. J. B. Clews, Acta Crystallogr. **26**, 693 (1970).
[29] Y. Delugeard, J. Desuche, and J. L. Baudour, Acta Crystallogr. **32**, 702 (1976).
[30] K. N. Baker, A. V. Fratini, T. Resch, H. C. Knachel, W. W. Adams, E. P. Socci, and B. L. Farmer, Polym. Papers **34**, 1571 (1993).
[31] S. Guha, W. Graupner, R. Resel, M. Chandrasekhar, H. R. Chandrasekhar, R. Glaser, and G. Leising, Phys. Rev. Lett. **82**, 3625 (1999).
[32] J. L. Baudour, Y. Delugeard, and P. Rivet, Acta Crystallogr. **34**, 625 (1978).
[33] B. Kohler, S. Wilke, M. Scheffler, R. Kouba, and C. Ambrosch-Draxl, Comput. Phys. Commun. **94**, 31 (1996).
[34] M. Rubio, M. Merchan, E. Orti, and B. O. Roos, Chem. Phys. Lett. **234**, 373 (1995).
[35] S. Narioka, H. Ishii, K. Edamatsu, K. Kamiya, S. Hasegawa, T. Ohta, N. Ueno, and K. Seki, Phys. Rev. B **52**, 2362 (1995).
[36] E. Zojer, M. Knupfer, R. Resel, F. Meghdadi, G. Leising, and J. Fink, Phys. Rev. B **56**, 10 138 (1997).
[37] R. K. Khanna, Y. M. Jiang, B. Srinivas, C. B. Smithhart, and D. L. Wertz, Chem. Mater. **5**, 1792 (1993).
[38] H. O. Marcy, M. J. Rosker, L. F. Warren, B. A. Reinhardt, M. Sinclair, and C. H. Seager, J. Chem. Phys. **100**, 3325 (1994).
[39] C. Ambrosch-Draxl, P. Puschnig, R. Resel, and G. Leising, Synth. Met. **101**, 673 (1999).
[40] H. Yanagi, S. Okamoto, and T. Mikami, Synth. Met. **91**, 91 (1997).